Elastic contact between randomly rough surfaces: Comparison of theory with numerical results

B. N. J. Persson,[1] F. Bucher,[2] and B. Chiaia[3]
[1]*IFF, FZ-Jülich, 52425 Jülich, Germany*
[2]*Technical University Berlin, Institute of Aeronautics and Astronautics, Marchstr. 12, 10587 Berlin, Germany*
[3]*Department of Structural and Geotechnical Engineering, Politecnico di Torino, Corso Duca degli Abruzzi 24, 10129 Torino, Italy*
(Received 23 July 2001; revised manuscript received 1 February 2002; published 29 April 2002)

One of us recently developed a theory of contact mechanics for randomly rough surfaces [B.N.J. Persson, J. Chem. Phys. **115**, 3840 (2001)]. In this paper we compare the results of the analytical model with (exact) numerical results. We also present some analytical results related to the theory.

DOI: 10.1103/PhysRevB.65.184106 PACS number(s): 81.40.Pq, 62.20.−x

I. INTRODUCTION

Even a highly polished surface has surface roughness on many different length scales. When two bodies with nominally flat surfaces are brought into contact, the area of real contact will usually only be a small fraction of the nominal contact area. We can visualize the contact regions as small areas where asperities from one solid are squeezed against asperities of the other solid; depending on the conditions the asperities may deform elastically or plastically.

How large is the area of *real* contact between a solid block and the substrate? This fundamental question has extremely important practical implications. For example, it determines the contact resistivity and the heat transfer between the solids. It is also of direct importance for sliding friction,[1] e.g., the rubber friction between a tire and a road surface, and it has a major influence on the adhesive force between two solids blocks in direct contact.

One of us recently developed a theory of contact mechanics,[2] valid for randomly rough (e.g., self-affine fractal) surfaces.[3] In the context of rubber friction, which motivated this theory, mainly elastic deformation occurs. However, the theory can also be applied when both elastic and plastic deformations occur in the contact areas. This case is, of course, relevant to almost all materials other than rubber.

In this paper we present results related to the theory,[2] and also numerical results, obtained by discretizing the basic equations of elasticity, to test the accuracy of the theory. We find that the theory is in good agreement with the numerical calculations. The analytical model, in addition to providing deeper insight into the nature of the area of contact, can, with only a small computational effort, be applied to surfaces with arbitrary surface roughness. As shown elsewhere,[2] the theory can also be applied to viscoelastic solids, and enters as an important ingredient in a theory of sliding friction recently developed for viscoelastic materials, e.g., rubber.[2]

The basic idea behind the contact theory is that it is very important not to *a priori* exclude any roughness length scale from the analysis. Thus if $A(\lambda)$ is the (apparent) area of contact on the length scale λ [more accurately, we *define* $A(\lambda)$ to be the area of real contact if the surface would be smooth on all length scales shorter than λ; see Fig. 1], then we study the function $P(\zeta)=A(\lambda)/A(L)$ which is the relative fraction of the rubber surface area where contact occurs on the length scale $\lambda=L/\zeta$ (where $\zeta\geqslant 1$), with $P(1)=1$. Here $A(L)=A_0$ denotes the macroscopic contact area [L is the diameter of the macroscopic contact area, so that $A_0 \approx L^2$].

We briefly review earlier work on contact mechanics. The paper by Hertz[4] gave the solution for the frictionless normal contact of two elastic bodies of quadratic profile. He found that the area of real contact varies nonlinearly with the load or squeezing force $\sim F_N^{2/3}$. In 1957 Archard[5] applied the Hertz solution to the contact between rough surfaces, and showed that for a simple fractal-like model, where small spherical bumps (or asperities) were distributed on top of larger spherical bumps and so on, the area of real contact varies *nearly linearly* with F_N. A similar conclusion was reached in Refs. 6–8, whose authors again assumed asperities with spherical summits (of identical radius) with a Gaussian distribution of heights. A more general contact mechanics theory was developed by Bush *et al.*[9,10] They approximated the summits by paraboloids and applied the classical Hertzian solution for their deformation. The height distribution was described by a random process, and they found that

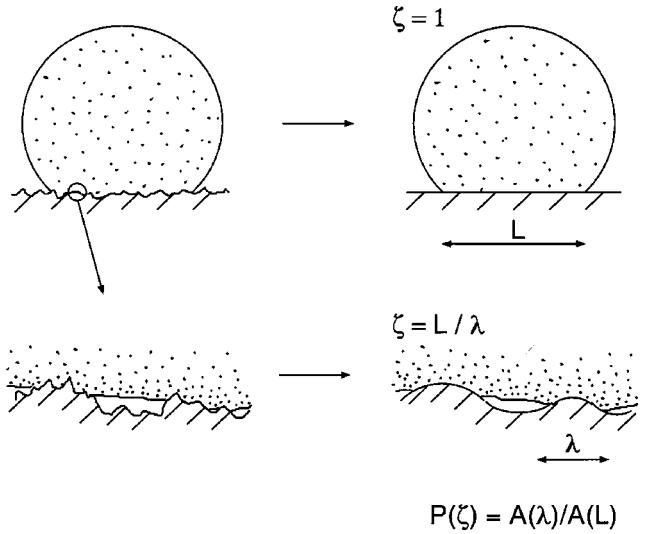

FIG. 1. A rubber ball squeezed against a hard, rough, substrate. Left: the system at two different magnifications. Right: The area of contact $A(\lambda)$ on the length scale λ is defined as the area of real contact when the surface roughness on shorter length scales than λ has been removed (i.e., the surface has been "smoothed" on length scales shorter than λ).

at low squeezing force the area of real contact increases linearly with F_N. The theory described below will be compared to the results of Bush *et al.* in Sec. IV.

II. THEORY

We briefly review the theory presented in Ref. 2. From contact mechanics (see, e.g., Ref. 8) it is known that in the frictionless contact of elastic solids with rough surfaces, the contact stresses depend only upon the shape of the gap between them before loading. Thus, without loss of generality, the actual system may then be replaced by a flat elastic surface [elastic modulus E and Poisson ratio ν, related to the original quantities via $(1-\nu^2)/E=(1-\nu_1^2)/E_1+(1-\nu_2^2)/E_2$] in contact with a rigid body having a surface roughness profile, which result in the same undeformed gap between the surfaces.

Consider a system at the length scale $\lambda=L/\zeta$, where L is of order the diameter of the nominal contact area. We define $q_L=2\pi/L$, and write $q=q_L\zeta$. Let $P(\sigma,\zeta)$ denote the stress distribution in the contact areas under the magnification ζ. The function $P(\sigma,\zeta)$ satisfies the differential equation (see Ref. 2):

$$\frac{\partial P}{\partial \zeta}=G'(\zeta)\sigma_0^2\frac{\partial^2 P}{\partial \sigma^2}, \tag{1}$$

where $G'(\zeta)$ denotes the ζ derivative of the function

$$G(\zeta)=\frac{\pi}{4}\left[\frac{E}{(1-\nu^2)\sigma_0}\right]^2\int_{q_L}^{\zeta q_L}dq q^3 C(q). \tag{2}$$

The surface roughness power spectra

$$C(q)=\frac{1}{(2\pi)^2}\int d^2x\langle h(\mathbf{x})h(0)\rangle e^{-i\mathbf{q}\cdot\mathbf{x}},$$

where $z=h(\mathbf{x})$ is the height of the surface above a flat reference plane (chosen so that $\langle h\rangle=0$), and $\langle\cdots\rangle$ stands for an ensemble average.

Let us write

$$P(\sigma,1)=P_0(\sigma).$$

If we assume a constant pressure in the nominal contact area, then $P_0(\sigma)=\delta(\sigma-\sigma_0)$.

Equation (1) is a diffusion-type equation, where time is replaced by the magnification ζ, and the spatial coordinate by the stress σ (and where the ''diffusion constant'' depends on ζ). Hence, when we study $P(\sigma,\zeta)$ on shorter and shorter length scales (corresponding to increasing ζ), the $P(\sigma,\zeta)$ function will become broader and broader in σ space. We can take into account that detachment will actually occur when the local stress reaches $\sigma=0$ (we assume no adhesion) via the boundary condition (see Appendix B)

$$P(0,\zeta)=0.$$

We assume that only elastic deformation occurs (i.e., the yield stress $\sigma_Y\to\infty$). In this case

$$P(\zeta)=\int_0^\infty d\sigma P(\sigma,\zeta).$$

It is straightforward to solve Eq. (1) with the boundary conditions $P(0,\zeta)=0$ and $P(\infty,\zeta)=0$ to obtain

$$P(\zeta)=\frac{2}{\pi}\int_0^\infty dx\frac{\sin x}{x}\exp[-x^2G(\zeta)]. \tag{3}$$

We now consider the limit $\sigma_0\ll E$, which is satisfied in most applications. In this case, for most ζ values of interest, $G(\zeta)\gg 1$, so that only $x\ll 1$ will contribute to the integral in Eq. (3), and we can approximate $\sin x\approx x$ and

$$P(\zeta)\approx\frac{2}{\pi}\int_0^\infty dx\exp[-x^2G(\zeta)]=[\pi G(\zeta)]^{-1/2}. \tag{4}$$

Thus, within this approximation, using Eqs. (2) and (4) we obtain $P(\zeta)\propto\sigma_0$, so that the area of real contact is proportional to the load.

The theory above is valid for surfaces with arbitrary random roughness, but will now be applied to self-affine fractal surfaces. It has been found that many ''natural'' surfaces, e.g., surfaces of many materials generated by fracture, can be approximately described as self-affine surfaces over a rather wide roughness size region. A self-affine fractal surface has the property that if we make a scale change that is different for each direction, then the surface does not change its morphology.[11] Recent studies have shown that even asphalt road tracks (of interest for rubber friction) are (approximately) self-affine fractal, with an upper cutoff length $\lambda_0=2\pi/q_0$ of the order of a few mm.[12] For a self-affine fractal surface $C(q)=C_0$ for $q<q_0$, while for $q>q_0$,

$$C(q)=C_0\left(\frac{q}{q_0}\right)^{-2(H+1)}, \tag{5}$$

where $H=3-D_f$ (where the fractal dimension $2<D_f<3$), and where q_0 is the lower cutoff wave vector, and C_0 is determined by the rms roughness amplitude, $\langle h^2\rangle=h_0^2/2$ via $C_0=\alpha(h_0/q_0)^2H/2\pi$ where $\alpha=1/[1+H-(q_L/q_0)^2H]$. Note that for $q_L/q_0\ll 1$, $\alpha\approx 1/(1+H)$ is independent of L.

Substituting Eq. (5) into Eq. (2), defining $q=q_L\zeta$ and assuming $q\gg q_0$ gives (also see Appendix A)

$$G(\zeta)\approx\left(\frac{q_0h_0}{4(1-\nu^2)}\right)^2\frac{\alpha H}{(1-H)}\left(\frac{E}{\sigma_0}\right)^2\left(\frac{q}{q_0}\right)^{2(1-H)},$$

so that

$$P(\zeta)\approx\frac{4(1-\nu^2)}{q_0h_0}\left(\frac{1-H}{\pi\alpha H}\right)^{1/2}\frac{\sigma_0}{E}\left(\frac{q}{q_0}\right)^{H-1}.$$

But $\sigma_0=F_N/A_0$, so that the (apparent) area of contact on the length scale $\lambda=2\pi/q$ becomes

$$A(\lambda)=A_0P(\zeta)=\frac{4(1-\nu^2)}{q_0h_0}\left(\frac{1-H}{\pi\alpha H}\right)^{1/2}\frac{F_N}{E}\left(\frac{\lambda}{\lambda_0}\right)^{1-H}. \tag{6}$$

If λ_1 denotes the low-distance cutoff in the self-affine fractal distribution (which cannot be smaller than an atomic dimen-

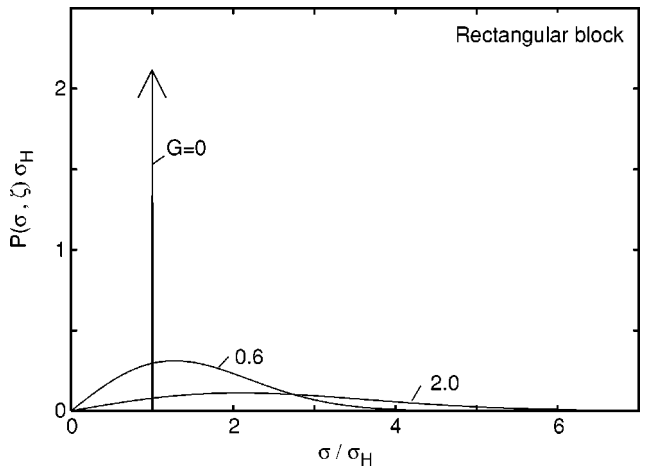

FIG. 2. The normal stress distribution in the contact area between a rectangular block and a nominally flat substrate. Here $\sigma_H=\sigma_0$ is the maximum stress in the contact area when $\zeta=1$. The pressure is shown for $G=0$, 0.6, and 2. The (apparent) contact area in the three different cases is A_0, $0.64A_0$, and $0.38A_0$.

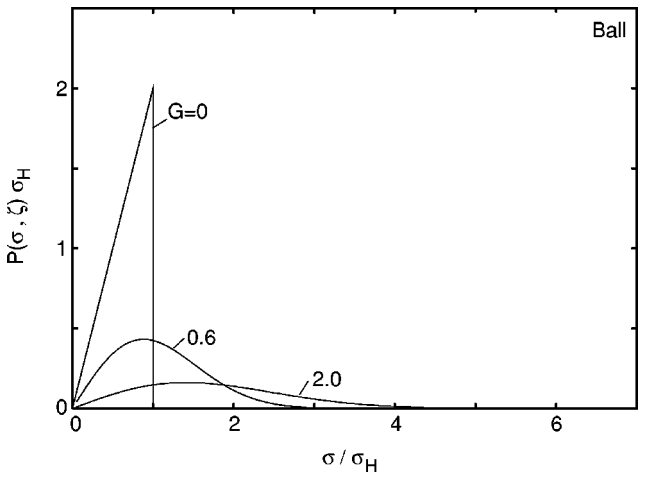

FIG. 3. The normal stress distribution in the contact area between a ball and a nominally flat substrate. The pressure is shown for $G=0$, 0.6, and 2. The (apparent) contact area in the three cases is A_0, $0.62A_0$, and $0.38A_0$.

sion), then Eq. (6) shows that the *area of real contact* $A(\lambda_1)$ is *proportional* to the load. We note that if the surface is self-affine fractal the whole way up to the lateral size L of the nominal contact area, then $q_0=2\pi/L$ and Eq. (6) predict that $A(\lambda)$ is proportional to L.

III. NUMERICAL RESULTS AND COMPARISON WITH OTHER CALCULATIONS

In this section we consider the stress distribution at the interface, assuming that only elastic deformation occurs. Assume first that a rectangular block with a nominally flat surface is squeezed against a nominally flat substrate. We neglect edge effects and assume the initial stress distribution

$$P(\sigma,1)=\delta(\sigma-\sigma_0),$$

where σ_0 is the average stress. The stress distribution for this case was calculated in Ref. 2,

$$P(\sigma,\zeta)=\sum_{n=1}^{\infty}\frac{2}{\sigma_Y}\sin\left(\frac{n\pi\sigma_0}{\sigma_Y}\right)\sin\left(\frac{n\pi\sigma}{\sigma_Y}\right)\times\exp\left[-\left(\frac{n\pi}{\sigma_Y}\right)^2\sigma_0^2G(\zeta)\right],$$

where the elastic limit corresponds to $\sigma_Y\to\infty$ (in numerical calculations one can keep σ_Y finite but large). In Fig. 2 we show the stress distribution for $G=0$, 0.6, and 2. In the figure σ_H denotes the maximum stress in the macroscopic contact area, which in the present case equals the average stress σ_0 since the stress for $\zeta=1$ is constant.

Since the equation of motion for $P(\sigma,\zeta)$ is linear, we can obtain the stress distribution for any other $P(\sigma,1)=P_0(\sigma)$ via

$$P(\sigma,\zeta)=\sum_{n=1}^{\infty}\frac{2}{\sigma_Y}\int_0^{\sigma_Y}d\sigma' P_0(\sigma')\sin\left(\frac{n\pi\sigma'}{\sigma_Y}\right)\sin\left(\frac{n\pi\sigma}{\sigma_Y}\right)\times\exp\left[-\left(\frac{n\pi}{\sigma_Y}\right)^2\sigma_0^2G(\zeta)\right]. \quad (7)$$

Let us first consider a circular Hertzian contact as arises, e.g., if a spherical elastic body is squeezed against a nominally flat substrate. We have

$$\sigma(\mathbf{x})=\sigma_H\left[1-\left(\frac{r}{r_H}\right)^2\right]^{1/2}, \quad (8)$$

where $L=2r_H$ is the diameter of the contact area and σ_H the maximum (macroscopic) contact pressure. The corresponding stress probability distribution function is

$$P(\sigma,1)=\frac{1}{\pi r_H^2}\int d^2x\,\delta[\sigma-\sigma(\mathbf{x})]=\frac{2\sigma}{\sigma_H^2} \quad (9)$$

for $\sigma<\sigma_H$, and zero otherwise. Note that the average pressure $\sigma_0=2\sigma_H/3$. The $G=0$ curve in Fig. 3 shows this stress distribution. Substituting Eq. (9) into Eq. (7) gives

$$P(\sigma,\zeta)=\sum_{n=1}^{\infty}\frac{2}{\sigma_Y}B_n\sin\left(\frac{n\pi\sigma}{\sigma_Y}\right)\exp\left[-\left(\frac{n\pi}{\sigma_Y}\right)^2\sigma_0^2G(\zeta)\right], \quad (10)$$

where

$$B_n=2\left(\frac{\sin\gamma_n}{\gamma_n^2}-\frac{\cos\gamma_n}{\gamma_n}\right)$$

and where $\gamma_n=n\pi\sigma_H/\sigma_Y$. The resulting stress distribution is shown in Fig. 3 for $G=0$, 0.6, and 2.

Finally, let us consider a cylinder squeezed against a nominally flat substrate. In this case the macroscopic pressure in the nominal contact region is of the Hertz form

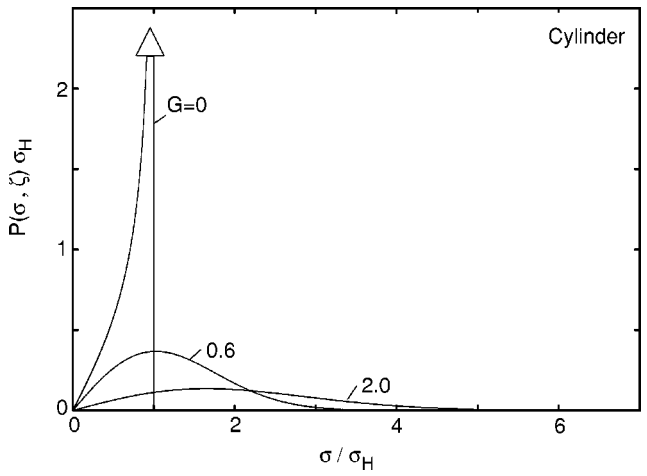

FIG. 4. The normal stress distribution in the contact area between a cylinder and a nominally flat substrate. The pressure is shown for $G=0$, 0.6, and 2. The (apparent) contact area in the three different cases is A_0, $0.61A_0$, and $0.37A_0$.

$$\sigma(x)=\sigma_H\left[1-\left(\frac{x}{a_H}\right)^2\right]^{1/2}, \tag{11}$$

where $L=2a_H$ is the width of the contact area and σ_H the maximum (macroscopic) contact pressure. The corresponding stress probability distribution is

$$P(\sigma,1)=\frac{1}{2a_H}\int_{-a_H}^{a_H}dx\,\delta[\sigma-\sigma(x)]=\frac{\sigma}{\sigma_H^2}\left[1-\left(\frac{\sigma}{\sigma_H}\right)^2\right]^{-1/2} \tag{12}$$

for $\sigma<\sigma_H$, and zero otherwise. Note that the average pressure $\sigma_0=\pi\sigma_H/4$. The $G=0$ curve in Fig. 4 shows this stress distribution. Substituting Eq. (12) into Eq. (7) gives $P(\sigma,\zeta)$ of the form of Eq. (10), with

$$B_n=\int_0^1 dx\;\; x(1-x^2)^{-1/2}\sin(\gamma_n x)$$

where $\gamma_n=n\pi\sigma_H/\sigma_Y$. Figure 4 shows the stress distribution for $G=0$, 0.6, and 2.

Bucher *et al.* studied the contact between a rail and wheel using a numerical method which is essentially exact when the grid size is made small enough.[13] The wheel is treated as a cylinder, and the rail as a nominally flat substrate occupying the xy plane. The two surfaces are randomly rough, and the contact is assumed to be purely elastic. To simplify the calculations, the asperities are assumed to have a constant height in the y direction, so that the deformation field is two-dimensional (the xz plane). The one-dimensional (1D)-power spectra $\overline{C}(q)$ is shown in Fig. 5, where q is measured in units of $(\mu\mathrm{m})^{-1}$ and $\overline{C}$ in units of $(\mu\mathrm{m})^3$:

$$\overline{C}(q)=\frac{1}{2\pi}\int dx\langle h(x)h(0)\rangle e^{-iqx}.$$

For a self-affine fractal surface, the 1D power spectra scales as $\sim q^{-2H-1}$ for $q>q_0$ [for the 2D power spectra the scaling is instead $\sim q^{-2H-2}$; see Eq. (5)]. From the slope (≈ -2) of

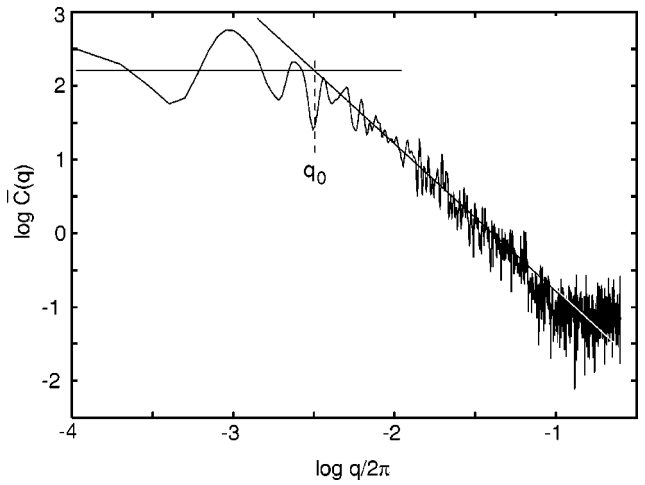

FIG. 5. The 1D roughness power spectra $\overline{C}(q)$ (for the combined wheel-rail system) as a function of the wave vector q of the surface roughness. For $q>q_0$, where $q_0\approx 2\times 10^4\mathrm{m}$, the power spectra $\overline{C}\sim q^{-2}$, corresponding to a self-affine fractal surface with the fractal dimension $D_\mathrm{f}\approx 2.5$. q is measured in units of $(\mu\mathrm{m})^{-1}$ and $\overline{C}$ in units of $(\mu\mathrm{m})^3$. Adapted from Ref. 13.

the curve for $q>q_0$, where $q_0\approx 2\times 10^4\mathrm{m}^{-1}$, we obtain $-2=-2H-1$ so that the roughness exponent $H\approx 0.5$ and the fractal dimension $D_\mathrm{f}=3-H\approx 2.5$.

Figure 6 shows the stress distribution as obtained from numerical calculations. If A_0 denotes the nominal contact area, then the area of contact at magnifications $\zeta=100$ and 400 becomes $\approx 0.62A_0$ and $0.33A_0$. Note that the stress distributions in Fig. 6 are similar to those in Fig. 4, and we can therefore compare the calculated contact areas (A_0, $0.61A_0$, and $0.37A_0$) with those obtained in the numerical study (A_0, $0.62A_0$, and $0.33A_0$) which are in relative good agreement.

In the numerical calculations by Bucher *et al.*, the width of the Hertzian contact area was $L=2a_H\approx 1$ cm, and the maximum Hertzian pressure $p_H=542$ MPa, giving an average pressure $\sigma_0\approx 426$ MPa. Using Eq. (6) with the elastic modulus $E=1\times 10^{11}$ Pa, $\nu=0.3$, and $h_0=0.95$ μm, at the magnification $\zeta=400$ (corresponding to $\lambda=0.0025$ cm) we obtain the area of real contact $\approx 0.2A_0$, which is relative close to the value obtained in the numerical study.

As a second example of contact between randomly rough surfaces, consider the results of Borri-Brunetto *et al.*[14] Using an essential exact numerical method, they studied how the area of contact depend on the magnification when a solid with a rough surface (self-affine fractal with the fractal dimension $D_f=2.3$) is squeezed against a flat substrate.

Figure 7 shows the area of contact, A, as a function of the applied load F_N (from Ref. 14). Results are presented for five different magnifications L/λ. Note that within the accuracy of the calculations, $A\sim F_N$. Also note that the slope of the curves decreases with increasing magnification; if we (arbitrarily) denote the slope for the magnification $L/\lambda=256$ with unity, then the slopes for $L/\lambda=128$, 64, 32, and 16 will be 1.24, 1.57, 1.93, and 2.32. This is in accordance with the theory presented above [see Eq. (6)], where the area of contact on the length scale λ is proportional to $A(\lambda)$

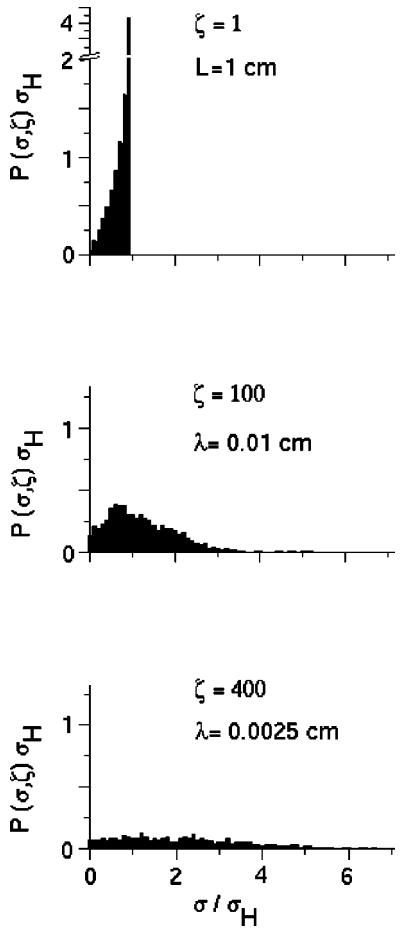

FIG. 6. The normal stress distribution in the contact area between a cylinder and a flat (model of rail-wheel contact problem). The Hertzian stress distribution extend over $L \approx 1$ cm. The stress distribution has been calculated numerically with 4999 grid points (see Ref. 13). The (apparent) contact area in the three different cases is A_0, $0.62A_0$, and $0.33A_0$.

$\sim(\lambda/L)^{1-H}$. Since $D_f=2.3$ we have $1-H=D_f-2=0.3$, so that the theoretical slopes are 1.23, 1.52, 1.87, and 2.30, in excellent agreement with the numerical results. Let us also compare the numerical value of the slope for magnification $L/\lambda=256$ with the theoretical prediction [Eq. (6)]. Since the surfaces are self-affine fractal the whole way up to the linear size of the contact area, we will take $q_0=2\pi/L$ in Eq. (6). We note that this expression for q_0 is somewhat uncertain, since L is the width of the square nominal contact area used in the computer simulations, while q_0 in the theory is a radial long-distance cutoff wave vector. Using the known elastic modulus (and Poisson ratio), the linear size of the contact area, and the rms roughness amplitude, we obtain the theoretical slope $6\times10^{-10}\mathrm{N}^{-1}$, to be compared to the slope in Fig. 7: $8\times10^{-10}\mathrm{N}^{-1}$.

Borri-Brunetto *et al.* also studied the dependence of A on the load (or normal force) F_N at a fixed magnification $L/\lambda=128$, for surfaces with three different fractal dimensions, namely, $D_f=2.1$, 2.3, and 2.5. They again observed a linear relation between A and F_N but with different slopes: if we (arbitrarily) denote the slope for $D_f=2.5$ with unity, then the slopes for $D_f=2.3$ and 2.1 will be 2.0 and 3.1. Using the expression for G derived in Appendix B (with $q_L=q_0$, since the generated surfaces where self-affine fractal right up to the lateral size of the nominal contact area) we obtain the theoretical slopes 1.8 and 3.0, again in good agreement with the numerical results. Finally, we note that if the surfaces are self-affine fractal the whole way up to the lateral size L of the nominal contact area, then $q_0=2\pi/L$ and Eq. (6) predict that $A(\lambda)$ (at a fixed magnification) is proportional to L. This is also in excellent agreement with our numerical studies.[15]

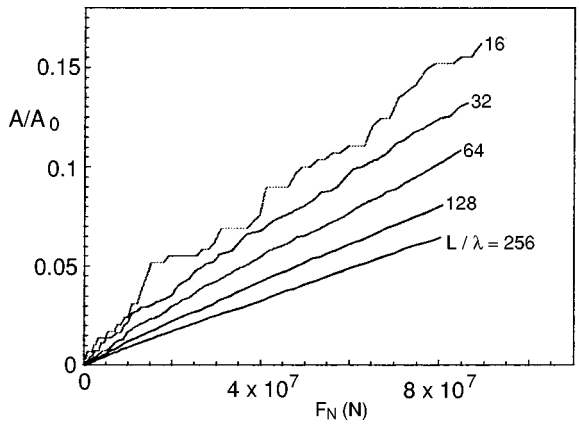

FIG. 7. The area of contact, A, as a function of the applied load F_N. Results are presented for five different magnifications L/λ. The fractal dimension is $D_f=2.3$. Adapted from Ref. 14.

IV. DISCUSSION

The present theory predicts that the area of contact increases linearly with the load for small load. In the standard theory of Greenwood and Williamson[7] this result holds only approximately and comparison of the prediction of their theory with the present theory is therefore difficult. Bush *et al.*[9] developed a more general and accurate contact theory, where the summits are approximated by paraboloids to which they apply the Hertzian contact theory. They found that at small load the area of contact depends linearly on the load according to

$$\frac{A}{A_0}=(1-\nu^2)\frac{F_N}{E}\left(\int_0^\infty dqq^3C(q)\right)^{-1/2}.$$

This result is very similar to the prediction of the present theory where, for a small load, from Eqs. (2) and (4),

$$\frac{A}{A_0}=\frac{2}{\pi}(1-\nu^2)\frac{F_N}{E}\left(\int_0^\infty dqq^3C(q)\right)^{-1/2}.$$

Thus our contact area is a factor of $2/\pi$ smaller than predicted by the theory of Bush *et al.* The theories of both Greenwood and Williamson and Bush *et al.*, assumed that the asperity contact regions are independent. However, as we show below, for real surfaces (which always have surface roughnesses on many different length scales) this will never be the case even at very low nominal contact pressures. We now argue that this may be the origin of the $2/\pi$ difference

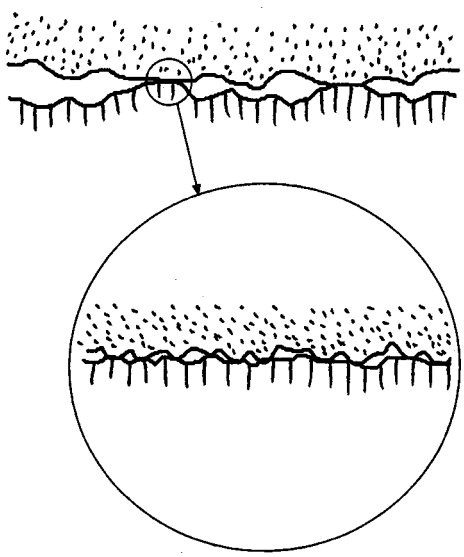

FIG. 8. The contact between two elastic solids. At a low nominal squeezing pressure, at the longest length scale λ_0 a low concentration of contact regions occurs, and the lateral (elastic) coupling between these macrocontact areas can be neglected. The (average) pressure in such a macrocontact area is independent of the applied pressure. The asperity contact regions within each macrocontact area will, on a short enough length scale, be so closely spaced that the lateral (elastic) interaction between these microasperity (or nanoasperity) contact regions must be taken into account.

between our theory (which assumes roughness on many different length scales) and the result of Bush *et al.*

Consider the contact between two solids at a very low nominal contact pressure. Consider first the system on the longest length scale λ_0. On this length scale the solids will make contact at a low concentration of (widely separated) contact areas; see Fig. 8. Since the separation between these *macro*contact areas is very large, we can neglect the interaction between the macrocontact areas; in this case the Greenwood-Williamson theory (and any other of the standard contact theories) predicts that the local contact pressure will be of order $\sim Eq_0h_0$. Thus the (average) pressure in the contact regions on the longest length scale is *independent* of the nominal contact pressure $\sigma_0 = F_N/A_0$. Now each macrocontact area is covered by smaller asperities, and the smaller asperities by even smaller asperities, and so on. It is easy to see that at a short enough length scale the small-asperity contact regions will be very closely separated, and it is therefore impossible to neglect the interaction between the asperities at short enough length scales. We now show that including the interaction between the small-sized asperities will tend to decrease the contact area in accordance with the result of our theory.

Consider two closely spaced asperities with spherical cups with identical radii of curvature but with different heights, as illustrated in Fig. 9. Assume that a flat rigid surface is squeezed against the rough surface. Let us first neglect the interaction between the asperities. If the flat surface makes contact with both asperities [see Fig. 9(a)], then according to Hertz contact theory the area of real contact is proportional to

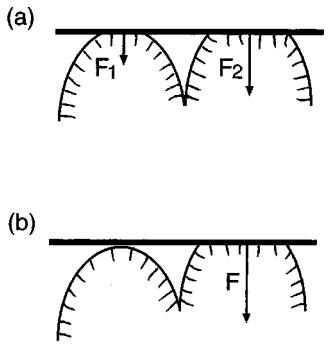

FIG. 9. Two closely spaced asperities squeezed against a hard flat wall with a force F. In (a) we have neglected the lateral (elastic) coupling between the asperities, and within this approximation the hard wall make contact with both the asperities, $F_1+F_2=F$. In (b) we have taken into account the lateral elastic coupling between the asperities. The force acting on the higher asperity results in a downward displacement of the lower asperity, so that no direct contact occurs between the lower asperity and the hard wall even when the total squeezing force F is the same as in (a).

$$A = a(F_1^{2/3} + F_2^{2/3}),$$

where F_1 and F_2 are the forces acting on the two asperities, and where a depends on the elastic modulus and the radius of curvature of the asperities. Let us now calculate the area of contact when the lateral interaction between the asperities is included. First note that, if we apply a force $F = F_1 + F_2$ to the higher asperity, this will not only compress this asperity but will also lower the other asperity as a result of the elastic deformation of the solid. We now assume that the resulting displacement of the lower asperity is so large that no contact occur with the rigid plane [see Fig. 9(b)]. Thus in this case the contact area is

$$A' = aF^{2/3} = a(F_1 + F_2)^{2/3} < A.$$

Thus, including the lateral interaction between the asperities will reduce the area of real contact. This effect is completely general, and not limited to the simple case studied above.

V. SUMMARY AND CONCLUSION

We have studied the contact stress distribution $P(\sigma,\zeta)$ and shown that $P(\sigma,\zeta) \sim \sigma$ as $\sigma \to 0$. The results for $P(\sigma,\zeta)$ of the analytical model has been compared with (exact) numerical results for the contact between a cylinder and a nominal flat substrate with surface roughness on many different length scales. The theory is in good agreement with the numerical results. The theory predicts that the area of contact in most cases varies linearly with the load, and that it depends on the magnification L/λ as $A(\lambda) \sim (\lambda/L)^{1-H}$; both predictions are in excellent agreement with (exact) numerical results.

ACKNOWLEDGMENTS

B.P. was supported by a research and development grant from Pirelli Pneumatici, and by a grant from BMBF related to the German-Israeli Project Cooperation ''Novel Tribologi-

cal Strategies from the Nano-to Meso-Scales.''

APPENDIX A: AREA OF CONTACT WITH A SMOOTH LONG-DISTANCE CUTOFF

Let us assume that $C(q)$ is given by

$$C(q)=C_0 \quad \text{for} \quad q<q_0$$

$$C(q)=C_0\left(\frac{q}{q_0}\right)^{-2(H+1)} \quad \text{for} \quad q>q_0$$

Substituting this into Eq. (2) gives

$$G=\beta C_0 q_0^4\left\{\frac{1}{4}\left[1-\left(\frac{q_L}{q_0}\right)^4\right]+\frac{1}{2(1-H)}\left[\left(\frac{q}{q_0}\right)^{2(1-H)}-1\right]\right\}, \tag{A1}$$

where

$$\beta=\frac{\pi}{4}\left[\frac{E}{(1-\nu^2)\sigma_0}\right]^2.$$

Thus, if $q_0 \gg q_L$ (i.e., $\lambda_0 \ll L$), the dependence of G on L is negligible.

APPENDIX B: BOUNDARY CONDITION FOR $\sigma=0$

We now prove that in the absence of adhesion, $P(\sigma,\zeta) \rightarrow 0$ as $\sigma \rightarrow 0$. Thus we are interested in $P(\sigma,\zeta)$ for small σ, which correspond to the contact regions close to the detached areas. We have

$$P(\sigma,\zeta)=\frac{1}{A_0}\int d^2x\,\delta[\sigma-\sigma_1(\mathbf{x})]$$

$$=\frac{1}{A_0}\sum_i \int_{A_i} d^2x\,\delta[\sigma-\sigma_1(\mathbf{x})],$$

where the sum is over all the asperity contact regions A_i (the contact will, in general, not consist of one single connected region but rather of many disconnected ''island'' regions). Now consider an arbitrary contact region A_i, see Fig. 10. In the absence of adhesion it can be shown that the local perpendicular stress vanishes as $\sigma_1(\mathbf{x}) \sim \xi^{1/2}$ as $\xi \rightarrow 0$, where ξ is the distance from the point $\mathbf{x}$ to the boundary line of the contact area A_i; see Fig. 10. (This is in contrast to the case when adhesion is included, where the stress instead diverge as $\xi^{-1/2}$ as $\xi \rightarrow 0$.) Let us introduce a curve-linear coordinate system (ξ,η), where the coordinate lines η are orthogonal to the coordinate lines ξ; see Fig. 10. Thus, for small ξ, we have $\sigma_1(\mathbf{x}) \approx g(\eta)\xi^{1/2}$, so that

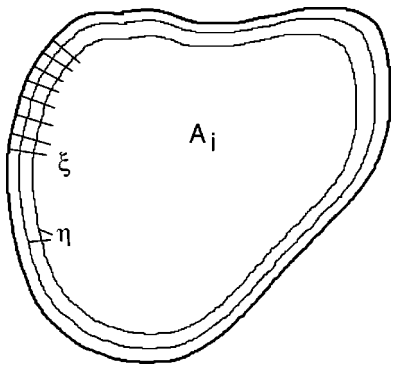

FIG. 10. Curve-linear coordinate system (ξ,η) in the contact area A_i. $\xi=0$ correspond to the boundary line of the contact region.

$$\int_{A_i} d^2x\,\delta[\sigma-\sigma_1(\mathbf{x})]=\int_{A_i} d\xi\,d\eta J(\xi,\eta)\,\delta[\sigma-g(\eta)\xi^{1/2}]$$

$$\approx \int d\eta \frac{2J(0,\eta)}{g^2(\eta)}\sigma, \tag{B1}$$

as $\sigma \rightarrow 0$. In Eq. (B1), $J(\xi,\eta)$ is the Jacobian of the coordinate transformation $(x,y) \rightarrow (\xi,\eta)$. Thus $P(\sigma,\zeta)$ vanishes *linearly* with σ as $\sigma \rightarrow 0$. Note that this result is consistent with the known results for Hertzian contact between a flat surface and a ball or a cylinder, where $P(\sigma,\zeta) \sim \sigma$ for $\sigma \ll \sigma_H$ [see Eqs. (9) and (12)].

[1] B. N. J. Persson, *Sliding Friction: Physical Principles and Applications*, 2nd ed. (Springer, Heidelberg, 2000).
[2] B.N.J. Persson, Phys. Rev. Lett. **87**, 1161 (2001); J. Chem. Phys. **115**, 3840 (2001).
[3] S. Roux, J. Schmittbuhl, J.P. Vilotte, and A. Hansen, Europhys. Lett. **23**, 277 (1993); A. Majumdar and B. Bhushan, J. Tribol. **113**, 1 (1991).
[4] H. Hertz, J. Reine Agnew. Math. **92**, 156 (1882).
[5] J.F. Archard, Proc. R. Soc. London, Ser. A **243**, 190 (1957).
[6] J. A. Greenwood, in *Fundamentals of Friction, Macroscopic and Microscopic Processes*, edited by I. L. Singer and H. M. Pollack (Kluwer, Dordrecht, 1992).
[7] J.A. Greenwood and J.B.P. Williamson, Proc. R. Soc. London, Ser. A **295**, 300 (1966).
[8] K.L. Johnson, *Contact Mechanics* (Cambridge University Press, Cambridge, 1985).
[9] A.W. Bush, R.D. Gibson, and T.R. Thomas, Wear **35**, 87 (1975).
[10] A.W. Bush, R.D. Gibson, and G.P. Keogh, Mech. Res. Commun. **3**, 169 (1976).
[11] J. Feder, *Fractals* (Plenum Press, New York, 1988).
[12] M. Klüppel and G. Heinrich, Rubber Chem. Technol. **73**, 578 (2000).
[13] F. Bucher, K. Knothe, and A. Theiler (unpublished).
[14] M. Borri-Brunetto, B. Chiaia, and M. Ciavarella, Comput. Methods Appl. Mech. Eng. **190**, 6053 (2001).
[15] B. Chiaia (unpublished).